Article

Not peer-reviewed version

Pseudomonas PA14H7: Identification of 7-Hydroxytropolone Iron Complex as a Potential Antagonist against Dickeya, the Causal Agent of Blackleg on Potato Plant

Euphrasie Munier-Lépinay , David Mathiron , Anthony Quéro , Mounia Khelifa , Sylvain Laclef * , Serge Pilard *

Posted Date: 12 July 2023

doi: 10.20944/preprints202307.0784.v1

Keywords: 7-hydroxytropolone; iron-complex; Pseudomonas; Dickeya; Pectobacteriaceae; Biocontrol; Blackleg; Soft Rot; Potato

Article

Pseudomonas PA14H7: Identification of 7-Hydroxytropolone Iron Complex as a Potential Antagonist against *Dickeya*, the Causal Agent of Blackleg on Potato Plant

Euphrasie Munier-Lépinay [1,2,3], David Mathiron [2], Anthony Quéro [4], Mounia Khelifa [1], Sylvain Laclef [3,*] and Serge Pilard [2,*]

[1] inov3PT-Recherche Développement Innovation des producteurs de plants de pomme de terre, 43-45 Rue de Naples, 75008 Paris, France; euphrasie.lepinay@inov3pt.fr; mounia.khelifa@inov3pt.fr
[2] Plateforme-analytique (PFA), Institut de Chimie de Picardie FR CNRS 3085, Université de Picardie Jules Verne, 33 rue Saint Leu, 80039 Amiens, France; david.mathiron@u-picardie.fr
[3] Laboratoire de Glycochimie, des Antimicrobiens et des Agroressources (LG2A), Institut de Chimie de Picardie FR CNRS 3085, Université de Picardie Jules Verne, 33 rue Saint Leu, 80039 Amiens, France; sylvain.laclef@u-picardie.fr
[4] UMRT INRAE 1158 BioEcoAgro (BioPI), UFR de Pharmacie, Université de Picardie Jules Verne, 1 rue des Louvels, 80037 Amiens cedex, France; anthony.quero@u-picardie.fr
* Correspondence: serge.pilard@u-picardie.fr; Tel.: +33-322-828-854, sylvain.laclef@u-picardie.fr, Tel.: +33-695-937-647

Abstract: Soft Rot Pectobacteriaceae (SRP) bacteria as *Pectobacterium* and *Dickeya* are phytopathogenic agents responsible of blackleg disease on several crop as potato, affecting the yield and depressing the seed production quality. However, neither conventional nor biocontrol product are available on the market to control this disease. In this study *Pseudomonas* PA14H7, a bacteria isolated from potato rhizosphere, was selected as a potential antagonist agent against *Dickeya*. In order to understand the mechanism involved in this antagonism we managed to identify the main active(s) molecule(s) produced by PA14H7. In that way, cell-free supernatant (CFS) of PA14H7 cultures were extracted and analyzed by LC-MS, GC-MS and NMR. We have correlated biological activity in extracted CFS-PA14H7 to the presence of 7-hydroxytropolone (7-HT) complexed with iron. Even if this molecule is produced by other *Pseudomonas* and mostly known for its antibacterial and antifungal activities, it is the first description of its involvement as an effective molecule against pectinolytic bacteria. We have synthesized 7-HT in order to determine the real amount produced by PA14H7 and to compare its activity at the same concentration with that of CFS-PA14H7. This study aims to understand the origin of the antagonist activity of PA14H7 as a potential biocontrol agent against potato blackleg.

Keywords: 7-hydroxytropolone; iron-complex; *Pseudomonas*; *Dickeya*; *Pectobacteriaceae*; biocontrol; blackleg; soft rot; potato

1. Introduction

Worldwide crops are subjected to a large panel of pests and diseases. Blackleg, also named soft rot when affecting tuber, is a bacterial disease caused by Soft Rot *Pectobacteriaceae* (SRP); from genus *Pectobacterium* or *Dickeya* [1,2] with a broad plant host spectrum. Moreover, contrary to other disease affecting potato, no treatments are available to control blackleg in vegetation and soft rot in conservation. Therefore those bacteria cause considerable economic losses mainly on potato crop [3], and are responsible of soft rot symptoms when developed on tuber [4].

Blackleg is induced by the macerating enzymes produced by SRP which degrade cell wall of potato plant. This process is led by virulence genes partially triggered by quorum-sensing (QS) mechanism [6]. The gene expression is coupled to bacterial cell concentration, and mediated by the diffusion of specific signal molecules. One of the best known QS-interrupting strategies is quorum-quenching (QQ) which involves the enzymatic degradation of these signal molecules. QQ strategy is

 doi:10.20944/preprints202307.0784.v1

effective on *Pectobacterium* [5,6] but not on *Dickeya* genus because its genes virulence is not relying only on QS mechanism [7].

Other strategies to control blackleg were also evaluated such as essential oils [8,9] or glycolipids-like compounds [10]. However these studies focused on controlling *Pectobacterium* as *P. atrosepticum* and not genus *Dickeya,* which is known as the most damaging pathogen causing blackleg [11].

The challenge was to find a biocontrol solution against both of the two genus responsible of the disease. Effort focused on the identification of bacteria which naturally colonized the same ecological niche than the pathogenic species [12]. Thus six bacteria were isolated from potato rhizosphere soil: *Pseudomonas fluorescens* PA3G8, *Pseudomonas brassicacearum* PA1G7 and PP1-210F, *Pseudomonas lactis* PA4C2, *Pseudomonas* sp. PA14H7 and *Bacillus simplex* BA2H3 [13]. Their antagonist activities were first evaluated against *Pectobacterium atrosepticum* and *Dickeya dianthicola* [13,14]. In a second step this evaluation was extended to a representative panel of *Pectobacterium* and *Dickeya* diversity in France, showing that PA14H7, as well as PA1G7 and PP1-210F have the greatest activity against SRP .

Nevertheless the origin of antagonism against SRP of the six bacteria previously cited, such as space competitivity or metabolite production [16], is not known. In this study we are looking for identification of secondary metabolites of interest in order to control blackleg disease caused by SRP. Indeed, *Pseudomonas* and *Bacillus* genus are known to produce a wide range of bioactive metabolites such as lipopeptides, phenazines, phloroglucinols, pyrroles, tropolones, volatile organic compounds. These molecules serve as antimicrobial agents, siderophores or biosurfactants [17–20].

In this study we evaluated the six bacteria antagonists against SRP using the cell-free supernatants (CFS) rather than direct bacterial confrontation. Indeed bacterial CFS has been reported to be potential source of biocontrol agents useful in sustainable agriculture [21]. The bacteria showing the most efficient activity was selected and its main active metabolite was characterized using Liquid Chromatography coupled to Mass Spectrometry (LC-MS), Gas Chromatography coupled to Mass Spectrometry (GC-MS) and Nuclear Magnetic Resonance (NMR) techniques. The metabolite was chemically synthesized in order to confirm its structure, its biological activity and was used as standard to quantify the amount produced by the bacteria in its CFS (Ultra-Violet (UV), LC-UV, LC-MS and GC-MS).

2. Results & Discussion

In order to identify the metabolite(s) responsible for antagonist's activity against pathogens causing potato blackleg, an approach based on extraction procedures, analytical methods and biological tests was designed.

In this study we will describe the different steps leading to the selection of the most efficient antagonist against SRP (Figure 1). The structural characterization and the quantification of the main active metabolite, produced in the CFS, responsible for its bactericidal/bacteriostatic activities, were conducted. Finally, comparison with the synthetic molecule was performed.

Preprints (www.preprints.org) | NOT PEER-REVIEWED | Posted: 12 July 2023 doi:10.20944/preprints202307.0784.v1

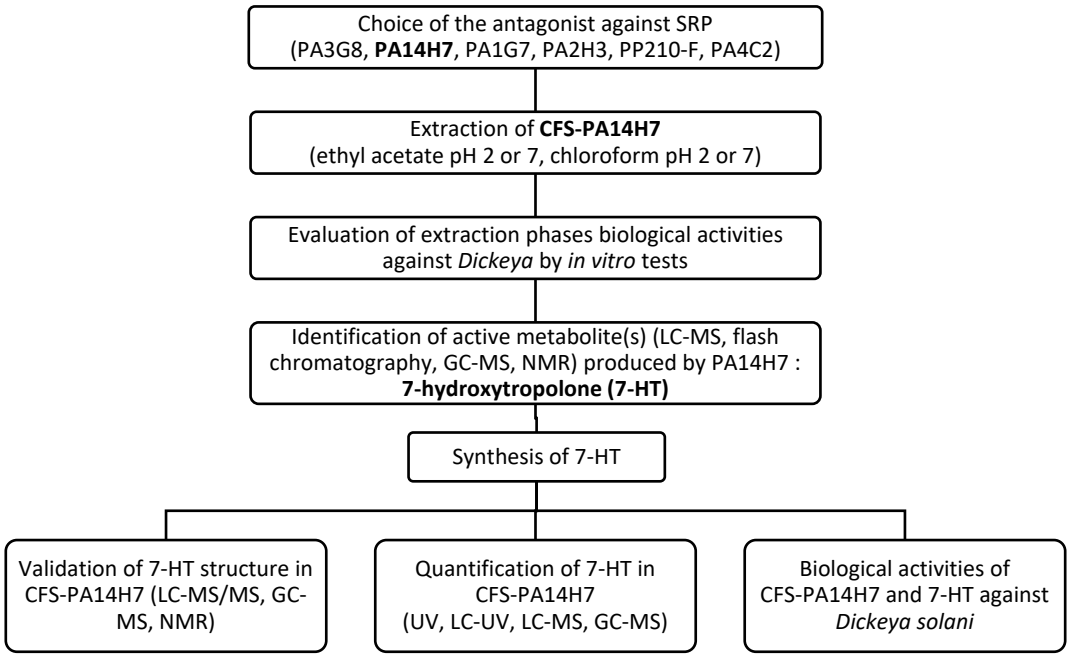

Figure 1. Flowchart of the approach for the selection of an efficient antagonist against SRP, causal agents of potato blackleg. Identification, quantification and evaluation of the biological activity of the main metabolite produced by this antagonist.

2.1. Choice of the main active antagonist

In order to find active metabolite to control SRP, we tested CFS obtained from bacteria grown in TY (Tryptone and Yeast extract) [21], a liquid nonselective rich media known to promote bacteria metabolite production [22]. CFS of selected bacteria: *Bacillus simplex* BA2H3, *Pseudomonas brassicacearum* PP1-210F and PA1G7, *Pseudomonas sp.* PA14H7, *Pseudomonas fluorescens* PA3G8, and *Pseudomonas lactis* PA4C2 [14] were confronted to a broad range of SRP (Table 1).

CFS of PA14H7, PA1G7 and PP1-210 showed a bactericidal effect against *P. atrosepticum* P8-Me25a (Table 1). These three bacteria had already presented a large scale inhibition effect against SRP, during direct confrontation *in vitro* tests [15]. However, CFS of PA14H7 was the only one showing a bacteriostatic effect against the whole tested panel of SRP (Table 1). In light of these results, PA14H7 seemed to be the best candidate able to produce active metabolite(s) against a broad range of SRP and so to be a suitable biocontrol agent in our strategy of controlling blackleg disease.

Table 1. Antagonistic effect of the selected bacteria CFS on growth of SRP from genus *Pectobacterium* and *Dickeya*.

	Antagonist bacteria strains					
SRP strains	**PA3G8**	**PA1G7**	**PA4C2**	**PA14H7**	**PA2H3**	**PP1-210F**
***P. atrosepticum* P8-Me25a**	-	++	-	++	-	++
***P. parmentieri* P13-CH22**	-	-	-	+	-	-
***P. brasiliense* P1-15C1**	-	-	-	+	-	-
***P. polaris* P1-10C1**	-	-	-	+	-	-
***D. dianthicola* P15-29**	-	-	-	+	-	-
***D. solani* P5-Sp1a**	-	-	-	+	-	-
***D. solani* 3337**	-	-	-	+	-	-

[1] The effect of CFS of antagonists PA3G8, PA1G7, PA4C2, PA14H7 PA2H3 and PP1-210F is marked "-" if no growth inhibition of pectinolytic bacteria is observed, "+" for bacteriostatic effect and "++" for bactericidal effect.

 doi:10.20944/preprints202307.0784.v1

2.2. Evaluation of CFS-PA14H7 extraction methods

After the selection of the antagonist, the second step was to determine when the bacteria reached the highest cell density, in order to maximize the chance of detecting and identifying potential metabolites. We carried out a kinetic experiment showing that the bacteria growth reached the stationary phase after 48 h of PA14H7 incubation (Supplementary material Figure S1). This time of incubation was used for all the upcoming steps.

We firstly attempt to directly analyzed the CFS-PA14H7 compared to TY medium alone. Unfortunately, the complexity of the LC-MS chromatograms, partly due to the composition of the medium (Supplementary material Table S1), did not allow us to point out major differences (Supplementary material Figure S2). We therefore designed different extractions with commonly used solvents (chloroform and ethyl acetate, at pH 2 and pH 7), in order to simplify the chromatogram analysis and to recover a maximum of metabolites. The LC-MS chromatograms of aqueous phases (Supplementary material Figure S3) and organic phases (Supplementary material Figure S4) were quite similar whatever the extraction method used. Consequently, we attempted to differentiate the efficient phases by achieving bioassays. *In vitro* tests were performed to evaluate their bacteriostatic and bactericidal activity against a strain of *Dickeya solani*, a major damageable pathogen affecting potato (Table 2 and Supplementary material Table S2).

Table 2. Comparison of biological activity against *Dickeya solani* 3337 of aqueous and organic phases obtained from the different extraction conditions of CFS-PA14H7.

		Aqueous phase (dilution factor)						**Organic phase (dilution factor)**					
Extraction conditions		**1**	**0.5**	**0.25**	**0.1**	**0.05**	**0.01**	**1**	**0.5**	**0.25**	**0.1**	**0.05**	**0.01**
Ethyl acetate	**pH 2**	-	-	-	-	-	-	++	++	++	++	++	-
	pH 7	-	-	-	-	-	-	++	++	++	++	+	-
Chloroform	**pH 2**	-	-	-	-	-	-	++	++	++	++	++	-
	pH 7	-	-	-	-	-	-	++	++	+	+	+	-

[1]"-" no effect "+" for bacteriostatic effect and "++" for bactericidal effect. Dilution 1 corresponds to an extraction of 300 mL CFS-PA14H7 concentrated 30 times.

The absence of antagonist effect of aqueous phases indicate that active metabolite(s) is only present in organic phases which have shown a similar efficiency whatever solvent and pH used for extraction.

2.3. Identification of the active metabolite(s)

2.3.1. LC-MS analysis

To identify the active metabolite(s) a comparison between the LC-MS profiles of TY versus CFS-PA14H7 organic phases after extractions was carried out. For all extractions, the organic phase chromatograms highlighted a major difference corresponding to a very large peak diffusing from 3.80 to 4.40 min, as exemplified for the chloroform extraction at pH 7 (Figure 2). We can notify that this peak coelute with another one at 4.01 min also present in the TY extract.

Preprints (www.preprints.org) | NOT PEER-REVIEWED | Posted: 12 July 2023 doi:10.20944/preprints202307.0784.v1

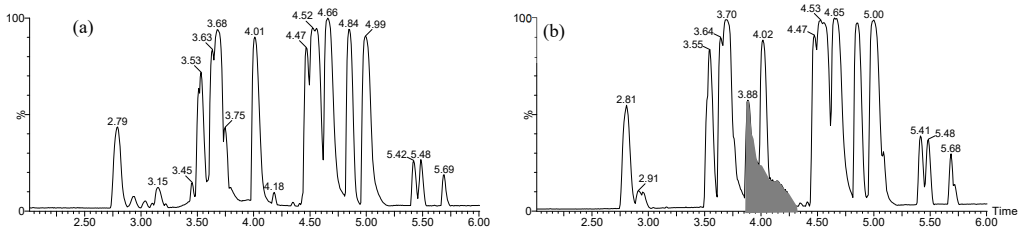

Figure 2. LC-MS (electrospray ionization in the positive ion mode: ESI^+), base peak intensity (BPI) chromatograms of organic phases after extraction with chloroform at pH 7 of TY culture medium (a) and CFS-PA14H7 (b). The major difference observed between 3.80 and 4.40 min is highlighted.

The mass spectrum corresponding to this large peak is presented in Figure 3a. It was mainly constituted of three ions at m/z 139.040, 329.983 and 658.957. These ions could be attributed to the same organic molecule: alone ($[M+H]^+$, $C_7H_6O_3$, m/z 139.040), as a dimeric complex with iron ($[2M-2H+Fe]^+$, $C_{14}H_{10}O_6Fe$, m/z 329.983) and its corresponding dimer generated at high concentration in the gas phase ($C_{28}H_{19}O_{12}Fe_2$, m/z 658.957). This phenomenon is evidenced by the reconstituted ionic current (RIC) traces of the different species presented Figure 3b.

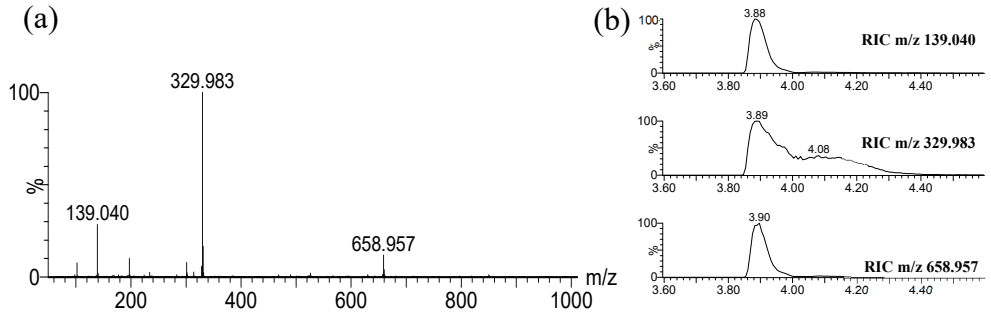

Figure 3. Mass spectrum of the large chromatographic peak observed between 3.80 and 4.40 min on the LC-MS BPI trace of CFS-PA14H7 chloroform extract (a). The RIC of the ions observed at m/z 139.040, 329.983 and 658.957 are also presented (b).

The complex with iron was established by the characteristic isotopic pattern distribution of $^{56}Fe/^{54}Fe$ (Figure 4). The distorted aspect of its chromatographic peak (RIC, m/z 329.983, Figure 3b) is also specific of a complex which is in equilibrium between its free and associated forms.

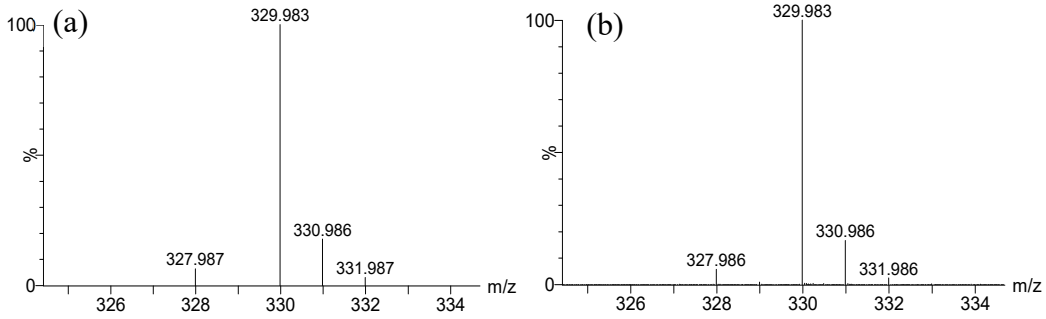

Figure 4. Theoretical isotopic pattern of elemental composition $C_{14}H_{10}O_6Fe$ (a) vs. experimental isotopic pattern of m/z 329.983 (b).

Specific research of accurate mass (m/z 139.040 and m/z 329.983, ± 20 ppm) revealed that neither the molecule nor its iron complex were present in TY, even in trace amount (Supplementary material Figure S5).

Finally, using the LC-MS data (retention time, m/z), we carried out a non-targeting profiling approach in order to identify all markers differentiating the culture medium TY from CFS-PA14H7.

Preprints (www.preprints.org) | NOT PEER-REVIEWED | Posted: 12 July 2023 doi:10.20944/preprints202307.0784.v1

This analysis revealed that the iron complex (m/z 329.983) and the free molecule (m/z 139.040) were clearly the main abundant markers generated in the presence of PA14H7 (Supplementary material Table S3).

2.3.2. Biologically driven purification using flash chromatography

In order to separate and isolate the active molecule from the rest of the chromatogram, we carried out a flash chromatography on a 3 liters chloroform pH 7 extraction of CFS-PA14H7. The evaporation of the solvent provided 156.22 mg of a brownish oil which was purified on a C18 reverse phase column. The purification process was monitored using UV wavelength at 244 and 320 nm. The latter correspond to the two maximums of absorbance, recorded by the Diode Array Detector (DAD), of the large peak eluting between 3.80-4.40 min during the LC-MS analysis (Figure 2 and Supplementary material Figure S6).

The flash chromatography fraction (F2) containing the peak detected in UV at 244 and 320 nm was collected (Supplementary material Figure S7), affording after evaporation 7.5 mg of a yellow powder. Fractions before (F1) and after (F3) the peak were also collected. The three fractions were biologically tested to confirm that the active metabolite is mainly present in F2. Fraction F1 did not show any biological activity contrary to fraction F3, which exhibited a reduced bactericidal/bacteriostatic effect probably due to the tailing of the peak collected in F2 (Table 3).

Table 3. Bacteriostatic/bactericidal effect against *Dickeya solani* 3337 of the flash chromatography fractions obtained after purification of a 3 liters CFS-PA14H7 extraction.

	Dilution factor							
Fraction	**1**	**0.5**	**0.25**	**0.1**	**0.05**	**0.01**	**0.005**	**0.001**
F1	-	-	-	-	-	-	-	-
F2	++	++	++	++	++	+	+	-
F3	++	++	+	-	-	-	-	-

[1]"-" no effect "+" for bacteriostatic effect and "++" for bactericidal effect. Dilution 1 correspond to the collected fractions.

2.3.3. Determination of the metabolite structure

The fraction F2 obtained after flash chromatography was submitted to different analytical techniques. Its LC-MS chromatogram and the corresponding mass spectrum confirmed that the main product, which was isolated, corresponds to the iron complex described part 2.3.1 (Supplementary material Figure S8). For unambiguous identification of the organic part of the complex, a GC-MS analysis was performed (Figure 5a). Indeed, the temperatures used for GC injection and separation led to dissociation of the complex in the gas phase. The electronic ionization low resolution mass spectrum (EI, Figure 5b) pointed out a molecular ion $M^{+\cdot}$ at m/z 138 in accordance with the $[M+H]^+$ at m/z 139.040 observed in the electrospray ionization high resolution mass spectrum (ESI-HRMS). A research in the NIST library led to two structure hypotheses: 7-hydroxytropolone (7-HT) or 2-ethoxyphenol. Only the elemental composition of 7-HT ($C_7H_6O_3$) was compatible with the accurate mass measurement results obtained in ESI^+ ($C_7H_6O_3$ exp. m/z 139.0396 vs. th. m/z 139.0395 and $C_7H_5O_3FeC_7H_5O_3$ exp. m/z 329.9827 vs. th. m/z 329.9828). The EI spectrum of 7-HT coming from NIST library is presented Figure 5c and those of the other hypothesis in the supplementary material (Figure S9). In addition, we carried out ^1H and ^{13}C NMR experiments of F2 in $CDCl_3$ (Figure 5d-e and Supplementary material S10). Despite the presence of co-eluted impurities also detected in LC-MS and GC-MS, the chemical shifts of the main compound were attributed to 7-HT structure.

Preprints (www.preprints.org) | NOT PEER-REVIEWED | Posted: 12 July 2023 doi:10.20944/preprints202307.0784.v1

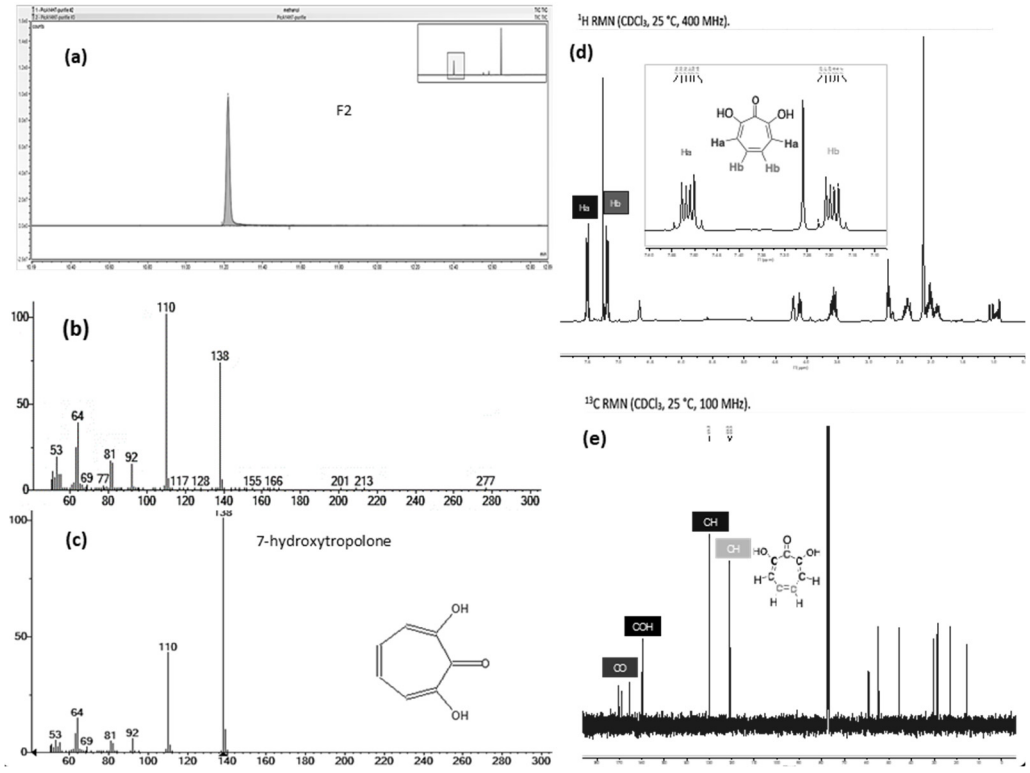

Figure 5. Analysis of the purified fraction F2 of CFS-PA14H7, after extraction (chloroform pH 7) and flash chromatography, by GC-MS (a) EI total ionic current (TIC) trace, (b) EI spectrum compared to (c) EI spectrum of 7-HT coming from NIST library, and NMR (d) ^{1}H NMR spectrum, (e) ^{13}C NMR spectrum.

2.4. Validation of 7-HT structure and activity

2.4.1. Organic synthesis of 7-HT

7-HT is not commercially available, and in order to unambiguously confirm its structure, its ability to form an iron complex and its activity, we carried out its synthesis in 4 steps from commercial tropolone, as previously described [23,24] (Supplementary material Figure S11). In that way 7.5 g of 7-HT was obtained from 25 g of tropolone corresponding to a yield of 27 %. NMR (Supplementary materials Figure S12) and GC-MS (Supplementary materials Figure S13) of the recrystallized synthetic 7-HT were in accordance with those obtained previously for the purified fraction F2. Nevertheless, in ^{1}H NMR spectrum in $CDCl_3$ of the purified extract we observed for the hydroxyl groups of tropolone moiety a broad singulet at 6.67 ppm integrating for 1 proton. For the synthetic 7-HT this singulet was shifted at 8.33 ppm and integrated for 2 protons. This phenomenon seems to indicate that 7-HT was present as a complex in CFS-PA14H7. An additional proof was obtained by injecting in LC-MS the synthetized 7-HT. As observed for CFS-PA14H7 extracts, 7-HT was detected as an iron complex at the same retention time and with identical MS/MS fragments ions, confirming that the entities we observed were the same (Figure 6).

Preprints (www.preprints.org) | NOT PEER-REVIEWED | Posted: 12 July 2023 doi:10.20944/preprints202307.0784.v1

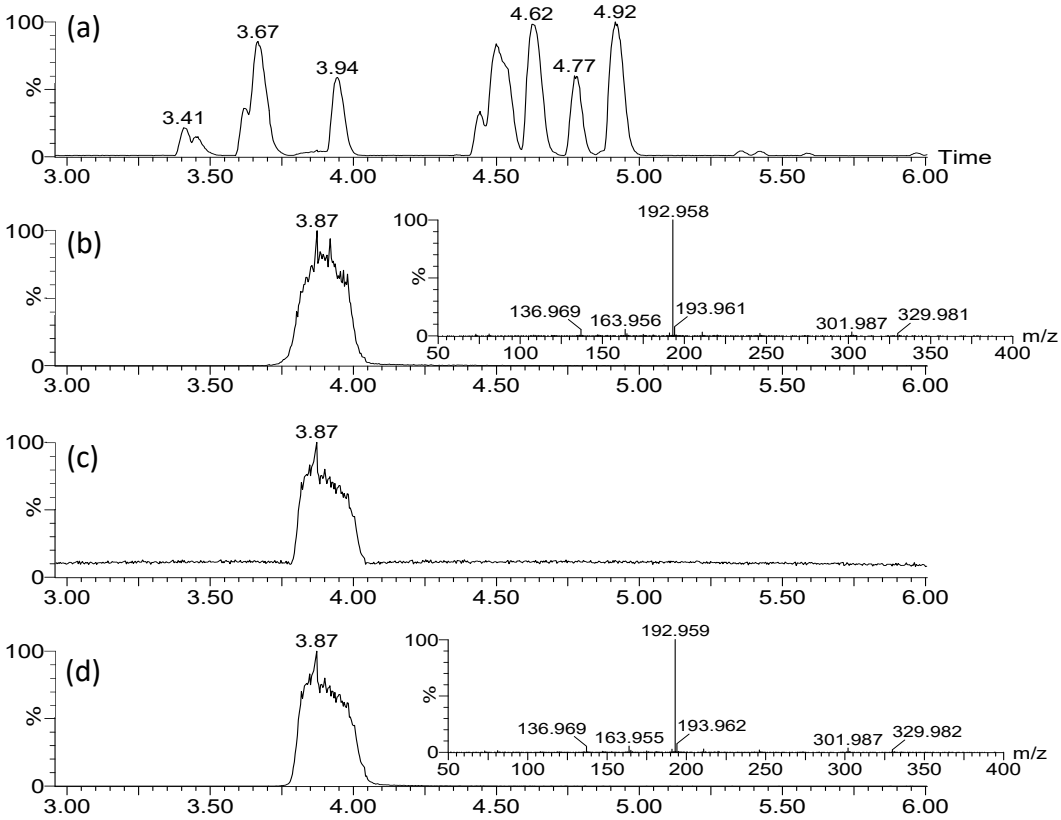

Figure 6. LC-MS/MS (ESI⁺) analysis of CFS-PA14H7 extracted with chloroform at pH7 : BPI (a) and RIC of m/z 329.983 with its corresponding MS/MS (30 eV) spectrum (b), compared with those of 7-HT obtained by synthesis (c) and (d).

The spectral data obtained by NMR and LC-MS indicate that 7-HT produced by PA14H7 form a complex with iron. The positive ion generated in ESI⁺ (m/z 329.983, Figure 3) revealed a 7-HT:iron(III) complex with a stoichiometric ratio of 2:1. A proposal structure for this complex and its MS/MS fragmentation pattern is depicted in Figure 7 and Supplementary material S14. The dimeric iron complex ion of 7-HT at m/z 329.982 gave rise after three successive losses of CO to the respective ions at m/z 301.987, 273.992 (very low intensity) and 245.997, which is consistent with the presence of carbonyl and hydroxyl groups on the 7-HT structure. Then the fragment ion at m/z 245.997 underwent fragmentation to give three ions at m/z 163.955, 136.968 and 81.033. The ion at m/z 163.955 could be explained by a catechol structure complexed with Fe(III) by losing from m/z 245.997 a hydroxy-cyclopentadiene molecule. The fragment at m/z 136.968 could come from the ion at m/z 245.997 by the loss of a catechol radical to give an hydroxy-cyclopentadiene structure complexed by Fe(II). The last of the three ions produced from m/z 245.997 at m/z 81.033 can be explained by the loss of a catechol structure complexed with Fe(III). Afterwards the fragment ion observed at m/z 210.968 can be obtained by two losses either a tropolone radical from the precursor ion at m/z 329.982 or a phenol radical from the fragment at m/z 301.987 to give the same monomeric radical ion of a 7-HT derivative always complexed by iron. The most abundant fragment ion at m/z 192.958 can be directly obtained from the precursor ion at m/z 329.982 by a loss of a hydroxy-tropolone radical leading to a monomeric hydroxy-tropolone ion with Fe(II). This behavior towards fragmentation directly evidences the dimeric nature of this complex as a homodimer. It should be noted that this hydroxy-tropolone radical loss involved a change in the oxidation state of iron with a reduction from Fe(III) to Fe(II). A loss of H_2O was observed from m/z 192.958 to give the ion at m/z 174.947. Finally, hydroxide anion complexed by Fe(II) at m/z 72.938 could potentially come from ions at m/z 192.958, 174.947 and 136.968. However, at this stage we were not able to determine the nature of the third ligand. One hypothesis could be another 7-HT molecule as described for ferric tropolone

Preprints (www.preprints.org) | NOT PEER-REVIEWED | Posted: 12 July 2023 doi:10.20944/preprints202307.0784.v1

characterized as a trimer of tropolone unit using single crystal X-ray diffraction [25], but other anions (sulfate, chloride, phosphate…) coming from growing medium are also possible.

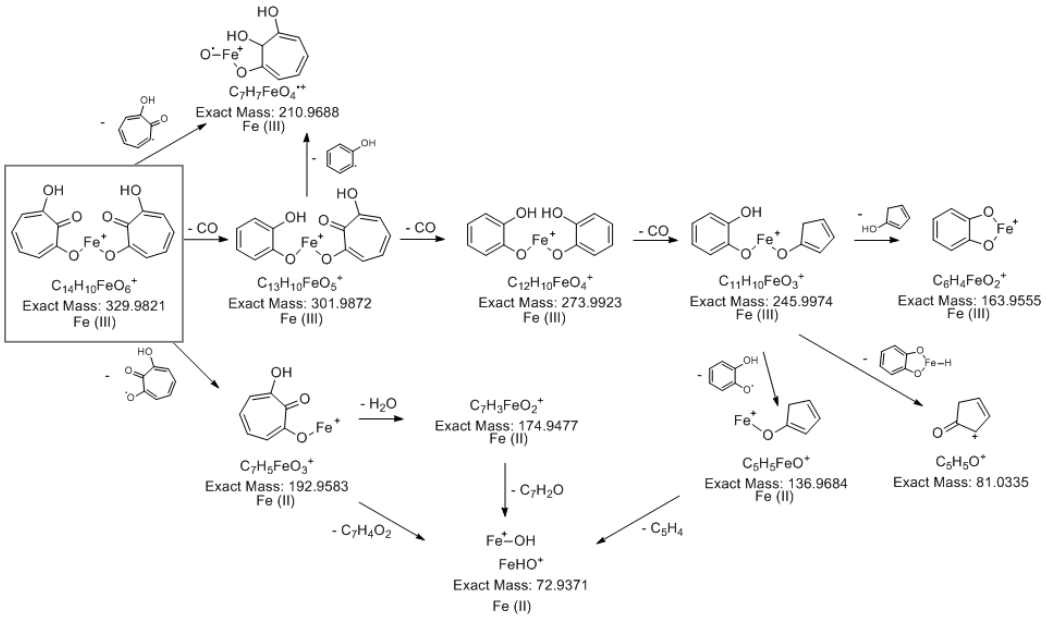

Figure 7. Proposal structure for the 7-HT:iron(III) 2:1 complex and its hypothetical fragmentation pattern obtained by MS/MS (30 eV).

2.4.2. Quantification of 7-HT produced by PA14H7

At this stage we have clearly identified 7-HT as the main active metabolite produced by PA14H7 in TY growth conditions. This result was in accordance with previously published results showing that 7-HT was already observed and identified as an iron chelator in different *Pseudomonas* strain such as *P. donguensis*, *P. qingdaonensis* and *P. wadenswilerensis* [20,26]. This natural molecule is well-known for its antibacterial and antifungal activities [27,28]. An important aspect was the possibility to accurately determine the amount produced by PA14H7, especially since 7-HT was complexed with iron in the culture medium.

The classical approach consists in a direct measurement of the UV absorbance at 327 nm in the CFS. The CFS-PA14H7 used for the determination of the amount of 7-HT produced by the bacteria revealed an OD_{327nm} of 1.02 and consequently a concentration in 7-HT of 14.2 mg/L (Supplementary material Figure S15). This result corresponded to specific growth conditions (initial concentration of bacteria, medium volume, incubation time). Indeed, when varying these conditions, we have observed OD_{327nm} ranging from 0.5 to 4 (corresponding to 7-HT concentration from 7 to 55 mg/L). That was in accordance with literature results, where 7-HT concentration values between 30 and 90 mg/L were determined using other bacterial strain [20,26]. This method is easy to implement and can be directly used on the CFS but it's not specific to 7-HT and can lead to an over-estimation due to the UV absorbance of other metabolites produced by the bacteria.

So, we decided to complete direct UV measurements with quantifications of CFS-PA14H7 extracts using LC-UV, LC-MS and GC-MS techniques which allowed the separation of 7-HT molecule from other species. The objective is to compare with the previous result (14.2 mg/L) and also to determine the level of recovery of the different extraction conditions. For each analytical method, the CFS-PA14H7 extracts were quantified using a calibration curve generated with the synthetic 7-HT (Supplementary material Figure S16). The results are listed in Table 4. Globally, concentrations in 7-HT were similar whatever the method used. Nevertheless, we can notify that recovery with ethyl acetate extraction at pH 7 was always lower than with other extraction methods even though we ensured that no 7-HT residue was detected in the aqueous phase.

Preprints (www.preprints.org) | NOT PEER-REVIEWED | Posted: 12 July 2023 doi:10.20944/preprints202307.0784.v1

Table 4. 7-HT measured concentration in CFS-PA14H7 (mg/L) for each extraction condition and processed using LC-UV (λ 320 nm), LC-MS (m/z 329.983) and GC-MS (m/z 138).

			Analytical methods		
	Extraction conditions		LC-UV	LC-MS	GC-MS
Extraction of CFS PA14H7[1]	Ethyl acetate	pH 2	8.9	8.5	12.4
		pH 7	5.7	6.0	7.3
	Chloroform	pH 2	7.9	8.2	10.0
		pH 7	10.3	8.5	8.9
Synthetic 7-HT in water (9.6 mg/L)	Ethyl acetate	pH 2	n.d.	8.9	9.7
	Chloroform	pH 7	n.d.	11.3	9.2

[1]Extraction and quantification were conducted on CFS-PA14H7 obtained from 1 L of PA14H7 culture in TY after 48 h incubation (value expressed in mg/L are a mean value obtained from three replicates).

Regarding these results, all extraction conditions, except for ethyl acetate pH 7, were acceptable for a good recovery of 7-HT in CFS. A value around 9 mg/L was determined, when averaging the three techniques, which is not so far from the direct UV measurement (14.2 mg/L). As a reference, synthesized 7-HT was diluted in water at 9.6 mg/L and extracted with chloroform at pH 7 and ethyl acetate at pH 2. The result depicted in Table 4 revealed that the extraction of 7-HT in water solution is complete. Concerning the analytical methods, GC-MS is the only technique which detect 7-HT as a non-iron complex molecule and is therefore the most suitable and reliable for integration/quantification due to a better chromatographic resolution, leading to a sharper chromatographic peak than those observed for the complexed form in LC-UV and LC-MS.

2.4.3. In vitro test of CFS-PA14H7 vs. synthetic 7-HT

To confirm that 7-HT is closely linked to the biological activity of CFS-PA14H7 it was necessary to establish the ability of the synthetic molecule alone to inhibit the *D. solani* growth. *In vitro* biological tests conducted in liquid medium at the concentration determined previously (9 mg/L) showed a similar inhibition effect on growth of *D. solani* than CFS-PA14H7 (Figure 8).

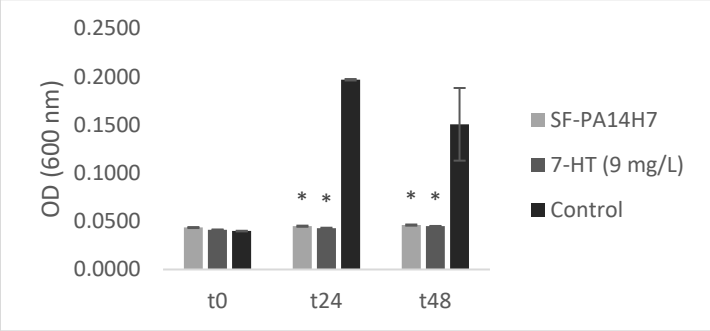

Figure 8. *Dickeya solani* growth in TY media containing CFS-PA14H7, 7-HT or water (control) measured by optical density. Bars are the mean value for three biological assays and the standard error are represented. (*) significant difference between the mean values compared to the control according to Kruskall-Wallis test at $p<0.05$.

To verify if the observed activities on *D. solani* were bacteriostatic or bactericidal, the liquid resulting of the incubation has been transferred on TY-agar Petri dishes. The growth of *D. solani* colonies for the two tested conditions shown that either 7-HT, or CFS-PA14H7 has only a bacteriostatic effect. This biological test is another proof that 7-HT identified in CFS-PA14H7 as an iron complex is involved in the antagonistic activity.

 doi:10.20944/preprints202307.0784.v1

3. Materials and Methods

3.1. Materials

For biological test, Bacto Tryptone and Bacto Yeast extract were provided by Fisher Scientific (Illkirch, France). Potassium phosphate mono, potassium phosphate dibasic and agar were purchased from Sigma Aldrich (Saint-Quentin, Fallavier, France).

For extraction, purification and chemical analysis, chloroform, ethyl acetate, methanol, formic acid, and water ULC-MS grade were purchased from Biosolve BV (Valkenswaard, The Nederlands. Hydrochloric acid solution 1M was purchased from Sigma Aldrich (Saint-Quentin, Fallavier, France). Deuterated reagent such as deuterated chloroform ($CDCl_3$) was purchased from Euriso-top (Saint-Aubin, France).

For organic synthesis, tropolone, 18-crown-6, iodomethane, N-bromosuccinimide, trifluoroacetic acid, acetic anhydride were purchased form Thermo Scientific (Illkirch, France). Benzene and toluene were purchased from Sigma Aldrich (Saint-Quentin, Fallavier, France).

3.2. Biological material

Bacillus simplex BA2H3, *Pseudomonas brassicacearum* PP1-210F and PA1G7, *Pseudomonas* PA14H7, *Pseudomonas fluorescens* PA3G8 and *Pseudomonas lactis* PA4C2 were previously isolated from potato soil rhizosphere [14,29]. *Dickeya solani* 3337 [30], *P. atrosepticum* P8-Me25a, *P. parmentieri* P13-CH22, *P. brasiliense* P1-15C1, *P. polaris* P1-10C1, *D. dianthicola* P15-29 and *D. solani* P5-Sp1a were previously isolated from potato blackleg symptom. All bacteria strains are stored at -80 °C in 25% glycerol for long time conservation. Before be used, bacterial strains were always revived on Petri dishes with TY_{agar}. All bacterial culture were inoculated at 1/1000 of their volume with a preculture of one colony into 5 mL of TY, and incubated at 27 °C, under agitation (130 rpm) for overnight to 48 h depending on the volume; (20 mL to 1 L). For antagonists strains, supernatant is obtained after 15 min centrifugation at 10 000 g and a filtration on 0.2 µm filter of the bacterial culture.

3.3. Biological test

Biological tests were conducted in microplate 96 well. There were filled with 80 µL of TY medium culture. 100 µL of filtered supernatant or synthesized molecule solution, at a known concentration were added and mixed to TY by pipetting. All solutions tested were realized in triplicates. Solution was replaced by sterilized water for blank. Finally, 20 µL of a solution of *Dickeya solani 3337* adjusted at 10^6 CFU/mL are inoculated. Bacteriostatic effect is observed by comparing the OD_{600nm} at 0 h, 24 h and 48 h of incubation at 27 °C and 130 rpm to the control condition. The bacterial concentration was first estimated by measuring OD at 600 nm with a Multiskan™ GO Microplate Spectrophotometer (Thermo Scientific, Illkirch, France). If no bacterial growth is observed after 48 h, the mix is spotted on TY-agar Petri dish and incubate at 27 °C. If colonies appear after 48 h, CFS has a bacteriostatic effect, if not, CFS has bactericidal effect.

3.4. Kinetics growth

A growth kinetics is realized on 1L of culture PA14H7 in TY medium incubated at 27°C and under 130 rpm agitation. Each hour, 1 mL medium is collected and OD at 600 nm is measured using multiskango®. 1 mL of TY medium free from inoculum is used as a blank.

3.5. Extraction method of CFS-PA14H7

300 mL of CFS-PA14H7 was prepared as previously described in 3.2 section. For extraction at pH 2, the pH was adjusted by addition of a solution of HCl (1M). The cell-free supernatant was then extracted with 3x100 mL of organic solvent (ethyl acetate or chloroform). Organic and aqueous phases were rotary evaporated. The organic resulting extract was resuspended in 10 mL of methanol, and the aqueous phase was diluted in 10 mL of water.

Preprints (www.preprints.org) | NOT PEER-REVIEWED | Posted: 12 July 2023 doi:10.20944/preprints202307.0784.v1

3.6. LC-UV-MS

Separations were performed using an ACQUITY UPLC H-Class system coupled on-line with an ACQUITY PDA detector and a Synapt G2-Si QTOF high-resolution hybrid mass spectrometer, equipped with an electrospray ionization (ESI) source (Z-spray) and an additional sprayer (Lock Spray) for the reference compound (Waters, Wilmslow, UK) The CFS-PA14H7 extracts and 7-HT standard were separated on an Acquity UPLC CSH C18 (1.7 µ 100 mm × 2.1 mm) chromatography column (Waters) maintained at 50 °C. The elution was performed using a 0.4 mL/min mobile phase gradient of water (A) and methanol (B), which both contained 0.1% formic acid, programmed, as follows (A:B): 90:10 (t = 0 min), 90:10 (t = 1 min), 10:90 (t = 7 min), 10:90 (t = 12 min), 90:10 (t = 13 min) and 90:10 (t = 18 min). Most of the time, 0.2 µL of each sample was injected. The UV acquisitions were performed using an in-line PDA detector ranging from 190 to 400 nm. 7-HT signal was processed at 320 nm for quantification. The ESI source was operated in positive ionization mode (ESI^+) using a capillary voltage of 3 kV. The following ESI source conditions were: sampling cone voltage, 40 V; source offset, 40 V; source temperature, 120 °C; desolvation gas temperature, 450 °C; desolvation gaz flow, 800 L/h; and, cone gas flow, 50 L/h. Nitrogen (>99.5%) was employed as the desolvation and cone gas. Mass calibration was carried out using a sodium formate solution (10mM NaOH in isopropanol/water/formic acid 49.9:49.9:0.2) and Leu-enkephalin (m/z 556.2771) was used as the lock mass solution for accurate measurements (1 ng/µL in H_2O/CH_3CN/Formic acid 50:49.9:0.1). The scan range was 50–2000 at 0.2 s/scan. The TOF was operated in the resolution mode (Resolution FWHM: 25,000). The HRMS spectra were recorded in the centroid mode. For quantification the reconstructed ionic current of the 7-HT iron complex ion (m/z 329.983) was integrated (window of 50ppm). For structural confirmation, MS/MS experiments were performed using a trap cell collision energy of 30 eV with argon (99.999%) as the collision gaz. Data acquisition and processing were performed using MassLynx software (V4.2, Waters).

3.7. Purification by Flash chromatography

3 L of CFS-PA14H7 were extracted with chloroform (3 x 1 L) at pH 7. After evaporation of the organic phase, the residue was dissolved in 2,5 mL of 80/20 methanol/water solution and subjected to flash chromatography separation on a Reveleris® PREP Purification System equipped with a FP ECOFLEX C18 12g column (BUCHI, Villebon-sur-Yvette, France). The elution was performed using a 30 mL/min mobile phase gradient of water (A) and methanol (B), programmed, as follows (A:B): 98:2 (t = 0 min), 98:2 (t = 2 min), 0:100 (t = 30 min) and 0:100 (t = 2 min). The detection was recorded using UV and Evaporative Light Scattering Detector (ELSD). The fractions of interest were collected using two wavelengths: 244 and 320 nm.

3.8. GC-MS

The CFS-PA14H7 extracts and 7-HT solutions prepared for LC-UV-MS analyses were also analyzed by GC-MS using a trace 1300 Gas Chromatograph coupled with an ISQ 7000 single quadrupole mass spectrometer (Thermo Scientific, San Jose, United States). 1 µL of each sample was injected using a 1:25 split ratio and an injector temperature of 230 °C. The temperature gradient started at 70 °C (5 min), then was increased at a speed of 15 °C/min during 23 min until reaching 310 °C (2 min). The column used for gas chromatography separation was a TR-5MS (length: 30m; inner diameter: 0.25 mm; film thickness: 0.25 µm) from Thermo Scientific. Helium was used as carrier gas at a flow rate of 1 mL/min. The electron impact (EI) ionization mode at 70 eV was used with a source temperature set to 280 °C. The mass spectra were recorded after a solvent delay of 5.5 min, using a mass range of 50 to 650 m/z at a rate of 0,. scan/sec. For identification of the 7-HT, the NIST library was used. For quantification, the reconstructed iron current of the molecular ion of 7-HT ($M^{+\cdot}$ m/z 138) was integrated and validated with a presence of 7-HT fragment at m/z 110. Acquisition and processing were performed with Chromeleon software, Version 7.2.

 doi:10.20944/preprints202307.0784.v1

3.9. NMR

^{1}H and ^{13}C nuclear magnetic resonance (NMR) spectra were recorded on an AVANCE III HD 400 MHz spectrometer (Brucker, Wissembourg, France) at 400 and 100 MHz, respectively. Chemical shifts are reported in parts per million (ppm) and spectra were calibrated using the non-deuterated residual solvent peak for $CDCl_3$ (^{1}H: δ=7.26 ppm, ^{13}C: δ=77.16 ppm). Peak multiplicity is reported as: singlet (s), doublet (d), doublet of doublet (dd), and broad (br). Acquisition was controlled by TopSpin 3.6.2 and the spectra were processed with Mestrenova 14.3.1. The spectra of 7-HT obtained by synthesis was used as a reference and compared to the CFS-PA14H7 spectra after extraction and purification (Supplementary material Figure S12). The detail of the 7-HT spectra is ^{1}H NMR ($CDCl_3$, 25 °C, 400 MHz): δ_H 8.33 br s, 2H), 7.51 (dd, J = 7.4, 3.8 Hz, 2H), 7.18 (dd, J = 7.4, 3.8 Hz, 2H). ^{13}C NMR ($CDCl_3$, 25 °C, 100 MHz): δ_C 168.9 (C), 159.9 (2xC), 129.8 (2xCH_2), 121.0 (2xCH_2).

3.10. Quantification of 7-HT

Calibration solutions of 7-HT were prepared by successive dilutions starting from a stock solution of synthesized 7-HT in methanol. The concentration range was established between 0.07 mg/mL and 0.56 mg/mL. Fresh mother solution and concentration range were prepared for each new series of measurements. For direct UV quantification on the CFS-PA14H7, and to be in the similar conditions measurement, the successive dilutions of 7-HT stock solution were realized in the growing medium TY. Firstly, UV spectra was recorded from 200 to 800 nm of synthesized 7-HT and CFS-PA14H7 with a Multiskan™ GO Microplate Spectrophotometer (Thermo Scientific, Illkirch, France). For concentration measurements, we selected the wavelength at 327 nm corresponding to the maximum of 7-HT absorbance. For the other quantification results obtained using hyphenated analytical methods (LC-UV, LC-MS, GC-MS) the data processing method is detailed in the material and method part related to the corresponding technique.

5. Conclusions

We identified that the Cell-Free Supernatant of PA14H7 has potent antagonist activity against Soft Rot *Pectobacteriaceae*. We demonstrated using the respective benefits of analytical techniques (LC-MS, GC-MS, NMR) and of *in vitro* biological tests that this activity was linked to the production in the CFS of 7-HT molecule complexed with iron. Quantification of 7-HT was achieved by direct UV measurements in CFS but also after a specific chromatographic separation by LC-UV, LC-MS and GC-MS in CFS extracts. GC-MS was determined to be the most reliable technique due to its higher chromatographic resolution. A detailed MS/MS study has shown the dimeric nature of this complex as a homodimer and has allowed to establish its structure and stochiometric to be 7-HT:iron(III) 2:1 complex. 7-HT has already been described in other *Pseudomonas* such as *P. donguensis* [26] and its ability to complex iron could be involved in the antagonistic activity against SRP by limiting access to iron for development of SRP. However, the comprehension of 7-HT mechanism of action needs further investigation. The cluster gene of 7-HT biosynthesis has been identified in *P. qingdaonensis* and *P. wadenswilerensis* [20]. In that way, the construction of a mutant deficient in 7-HT biosynthesis pathways will allow us to clearly establish if the antagonist activity is only due to this metabolite or if it exists another mechanism such as spatial competition as well as synergic effect with other metabolites. The mutant could also help to determine the essential precursor of 7-HT biosynthesis and can enable to increase 7-HT bioproduction by modulating the growing media compositions. Indeed it is known that the medium can affects metabolite production [31].

To limit pathogen propagation in general and the blackleg disease in particular, the use of biocontrol approach faced multiple issues. The successful transition from *in vitro* or greenhouse experiment to field condition are not often conclusive due to annual variation of climatic conditions, as humidity or temperature affecting survival and multiplication of biocontrol agent [32]. In order to reduce these abiotic influences, the use of active metabolites in addition to the biocontrol agent could be a possible solution [17]. In this context, it could be useful to develop a greener and faster synthesis

of 7-HT which is not marketed. The use of commercial analogous molecules able to form iron complex could also be investigated.

Supplementary Materials: The following supporting information can be downloaded at the website of this paper posted on Preprints.org. Figure S1. Growth kinetics of Pseudomonas PA14H7 in TY medium; Table S1. Detailed composition of Bacto Tryptone (named T); Figure S2. LC-MS (electrospray ionization in the positive ion mode: ESI+), base peak intensity (BPI) chromatograms of TY culture medium (A) and CFS-PA14H7 (B); Figure S3. LCMS (ESI+) comparison of TY culture medium (left) and CFS-PA14H7 (right) chromatograms of aqueous phases after extraction with chloroform at pH 7 (A), chloroform at pH 2 (B), ethyl acetate pH 7 (C) or ethyl acetate pH 2 (D); Figure S4. LC-MS (ESI+) comparison of TY culture medium (left) and CFS-PA14H7 (right) chromatograms of organic phases after extraction with chloroform at pH 7 (A), chloroform at pH 2 (B), ethyl acetate pH 7 (C) or ethyl acetate pH 2 (D). Extraction performed on the same batch of TY and PA14H7 filtered supernatant; Table S2. Results of bacteriostatic/bactericidal effect of organic and aqueous phases of CFS-PA14H7 extract with chloroform or ethyl acetate at pH 2 or pH 7; Figure S5: The reconstituted ion current (RIC) of the ions observed between 3.6 and 4.6 min at m/z 139.040 (A), m/z 329.983 (B) and m/z 658.957 (C) in TY culture medium (left) and CFS-PA14H7 (right); Table S3. Summary of markers present in CFS-PA14H7 and absent in TY medium analyzed with marker lynx (Waters, Masslynx V4.2); Figure S6. UV trace corresponding to the maximum of absorbance of the iron complex (B), absent in TY UV trace (A). Corresponding LC-MS (ESI+) BPI chromatograms for TY culture medium (C) and CFS-PA14H7 (D) highlighting the presence of the complex at m/z 329.983; Figure S7. Ultra-Violet (UV) at 224 nm (blue) and 320 nm (purple) and Evaporative Light Scattering Diffusion (ELSD) (green) chromatograms of the flash chromatography purification of CFS-PA14H7 using a C18 column. Fraction F1 is highlighted in green, F2 in orange, and F3 in blue; Figure S8 LC-MS (ESI+) chromatograms of fraction F2 resulting from CFS-PA14H7 purification by flash chromatography, BPI trace (A), RIC of the ions at m/z 139.040 (B) and m/z 329.983 (C). The purified iron complex is effectively detected between 3.80 and 4.40 min. The corresponding mass spectra are also depicted; Figure S9. EI NIST library spectra of the different hypothesis for the molecular ion observed at m/z 138. 7-HT (A) and 2-ethoxyphenol and isomers (B); Figure S10: Detailed NMR spectra of fraction F2 resulting from CFS-PA14H7 purification by flash chromatography: (A) 1H NMR (400 MHz) and (B) 13C NMR (100 MHz); Figure S11 : Synthesis of 7-hydroxytropolone starting from commercial tropolone; Figure S12: (A) 1H NMR and (B) 13C NMR spectra of 7-HT obtained by synthesis and (C) 1H NMR spectra and (D) 13C NMR spectra comparison of fraction F2 resulting from CFS-PA14H7 purification by flash chromatography (top) and synthetic 7-HT (bottom) between 6.3 and 9.1 ppm; Figure S13 : GC-MS chromatograms and spectra of 7-HT obtained by synthesis (A, C) and of fraction F2 resulting from CFS-PA14H7 purification by flash chromatography (B, D); Figure S14 : Proposal fragmentation pattern of 7-HT iron complex ion (m/z 329.983) by MS/MS (30 eV); Figure S15 : (a) UV spectrum of CFS-PA14H7 (1L, 48h) and of 7-HT of various concentrations in solution in TY (b) calibration curve of 7-HT in TY solution, at 327 nm ranging from 1.4 to 27.6 mg/L; Figure S16 : Standard curve performed with 7-HT synthetic molecule range from 0.07 mg/mL and 0.56 mg/mL according to LC-UV (320nm) (A), LC-MS (m/z 329.983) (B) and GC-MS (m/z 138) analysis (C).

Author Contributions: M.K., S.L. and S.P. designed the experiments, E.M.L. carried out biologicals tests, E.M.L. and S.P. carried out extractions. D.M., E.M.L, S.P. and carried out the MS acquisitions and their interpretation. A.Q. carried out the GC-MS acquisitions and their analysis. E.M.L. and S.L. carried out the flash chromatography purification. S.L. carried out the 7-HT synthesis. D.M. and S.L. carried out the NMR acquisition and analysis. E.M.L., M.K., S.L. and S.P. wrote manuscript. All authors critically revised, read and approved the final version of manuscript.

Funding: We are grateful to Bernard Quéré, Director of inov3PT, for the financing of Euphrasie Munier-Lépinay phD in collaboration with the University of Picardie Jules Verne (UPJV).

Acknowledgments: We are grateful to Peggy Colson from inov3PT for its punctual technical support for bacterial test.

Conflicts of Interest: The authors declare no conflict of interest.

References

1. Pérombelon, M.C.M. Potato Blackleg: Epidemiology, Host-Pathogen Interaction and Control. *Netherlands Journal of Plant Pathology* **1992**, *98*, 135–146, doi:10.1007/BF01974480.
2. Toth, I.K.; Barny, M.; Czajkowski, R.; Elphinstone, J.G.; Li, X. (Sean); Pédron, J.; Pirhonen, M.; Van Gijsegem, F. *Pectobacterium* and Dickeya: Taxonomy and Evolution. In *Plant Diseases Caused by Dickeya and*

Pectobacterium Species; Van Gijsegem, F., van der Wolf, J.M., Toth, I.K., Eds.; Springer International Publishing: Cham, 2021; pp. 13–37 ISBN 978-3-030-61459-1.

3. Dupuis, B.; Nkuriyingoma, P.; Van Gijsegem, F. Economic Impact of Pectobacterium and Dickeya Species on Potato Crops: A Review and Case Study. In *Plant Diseases Caused by Dickeya and Pectobacterium Species*; Van Gijsegem, F., van der Wolf, J.M., Toth, I.K., Eds.; Springer International Publishing: Cham, 2021; pp. 263–282 ISBN 978-3-030-61459-1.
4. Van Der Wolf, J.M.; Acuña, I.; De Boer, S.H.; Brurberg, M.B.; Cahill, G.; Charkowski, A.O.; Coutinho, T.; Davey, T.; Dees, M.W.; Degefu, Y.; et al. Diseases Caused by Pectobacterium and Dickeya Species Around the World. In *Plant Diseases Caused by Dickeya and Pectobacterium Species*; Van Gijsegem, F., Van Der Wolf, J.M., Toth, I.K., Eds.; Springer International Publishing: Cham, 2021; pp. 215–261 ISBN 978-3-030-61458-4.
5. Cirou, A. Développement de Stratégies d'anti-Virulence Ciblant La Régulation Quorum-Sensing Chez *Pectobacterium atrosepticum*, Bactérie Pathogène de La Pomme de Terre. These de doctorat, Paris 11, 2010.
6. Cirou, A.; Mondy, S.; An, S.; Charrier, A.; Sarrazin, A.; Thoison, O.; DuBow, M.; Faure, D. Efficient Biostimulation of Native and Introduced Quorum-Quenching Rhodococcus Erythropolis Populations Is Revealed by a Combination of Analytical Chemistry, Microbiology, and Pyrosequencing. *Appl Environ Microbiol* **2012**, *78*, 481–492, doi:10.1128/AEM.06159-11.
7. Blin, P.; Robic, K.; Khayi, S.; Cigna, J.; Munier, E.; Dewaegeneire, P.; Laurent, A.; Jaszczyszyn, Y.; Hong, K.; Chan, K.; et al. Pattern and Causes of the Establishment of the Invasive Bacterial Potato Pathogen *Dickeya Solani* and of the Maintenance of the Resident Pathogen *D. Dianthicola*. *Mol Ecol* **2021**, *30*, 608–624, doi:10.1111/mec.15751.
8. Zomorodian, K.; Ghadiri, P.; Saharkhiz, M.J.; Moein, M.R.; Mehriar, P.; Bahrani, F.; Golzar, T.; Pakshir, K.; Fani, M.M. Antimicrobial Activity of Seven Essential Oils From Iranian Aromatic Plants Against Common Causes of Oral Infections. *Jundishapur J Microbiol* **2015**, *8*, e17766, doi:10.5812/jjm.17766.
9. Hajian-Maleki, H.; Baghaee-Ravari, S.; Moghaddam, M. Efficiency of Essential Oils against Pectobacterium Carotovorum Subsp. Carotovorum Causing Potato Soft Rot and Their Possible Application as Coatings in Storage. *Postharvest Biology and Technology* **2019**, *156*, 110928, doi:10.1016/j.postharvbio.2019.06.002.
10. Azaiez, S.; Ben Slimene, I.; Karkouch, I.; Essid, R.; Jallouli, S.; Djebali, N.; Elkahoui, S.; Limam, F.; Tabbene, O. Biological Control of the Soft Rot Bacterium Pectobacterium Carotovorum by Bacillus Amyloliquefaciens Strain Ar10 Producing Glycolipid-like Compounds. *Microbiological Research* **2018**, *217*, 23–33, doi:10.1016/j.micres.2018.08.013.
11. Toth, I.K.; van der Wolf, J.M.; Saddler, G.; Lojkowska, E.; Hélias, V.; Pirhonen, M.; Tsror (Lahkim), L.; Elphinstone, J.G. Dickeya Species: An Emerging Problem for Potato Production in Europe. *Plant Pathology* **2011**, *60*, 385–399, doi:10.1111/j.1365-3059.2011.02427.x.
12. de Weert, S.; Bloemberg, G.V. Rhizosphere Competence and the Role of Root Colonization in Biocontrol. In *Plant-Associated Bacteria*; Gnanamanickam, S.S., Ed.; Springer Netherlands: Dordrecht, 2006; pp. 317–333 ISBN 978-1-4020-4538-7.
13. Essarts, yannick R.D. Pathogénie de Dickeya dianthicola et Dickeya solani chez Solanum tuberosum, développement et évaluation de stratégies de lutte biologique. phdthesis, Université Paris Sud - Paris XI, 2015.
14. Raoul des Essarts, Y.; Cigna, J.; Quêtu-Laurent, A.; Caron, A.; Munier, E.; Beury-Cirou, A.; Hélias, V.; Faure, D. Biocontrol of the Potato Blackleg and Soft Rot Diseases Caused by Dickeya Dianthicola. *Applied and Environmental Microbiology* **2016**, *82*, 268–278, doi:10.1128/AEM.02525-15.
15. Cigna, J.; Robic, K.; Dewaegeneire, P.; Hélias, V.; Beury, A.; Faure, D. Efficacy of Soft-Rot Disease Biocontrol Agents in the Inhibition of Production Field Pathogen Isolates. *Microorganisms* **2023**, *11*, 372, doi:10.3390/microorganisms11020372.
16. Syed Ab Rahman, S.F.; Singh, E.; Pieterse, C.M.J.; Schenk, P.M. Emerging Microbial Biocontrol Strategies for Plant Pathogens. *Plant Science* **2018**, *267*, 102–111, doi:10.1016/j.plantsci.2017.11.012.
17. Mishra, J.; Arora, N.K. Secondary Metabolites of Fluorescent Pseudomonads in Biocontrol of Phytopathogens for Sustainable Agriculture. *Applied Soil Ecology* **2018**, *125*, 35–45, doi:10.1016/j.apsoil.2017.12.004.
18. Dimkić, I.; Janakiev, T.; Petrović, M.; Degrassi, G.; Fira, D. Plant-Associated Bacillus and Pseudomonas Antimicrobial Activities in Plant Disease Suppression via Biological Control Mechanisms - A Review. *Physiological and Molecular Plant Pathology* **2022**, *117*, 101754, doi:10.1016/j.pmpp.2021.101754.

19. Dowling, D.; O'Gara, F. Metabolites of Pseudomonas Involved in the Biocontrol of Plant Disease. *Trends in Biotechnology* **1994**, *12*, 133–141, doi:https://doi.org/10.1016/0167-7799(94)90091-4.
20. Muzio, F.M.; Agaras, B.C.; Masi, M.; Tuzi, A.; Evidente, A.; Valverde, C. 7-hydroxytropolone Is the Main Metabolite Responsible for the Fungal Antagonism of *Pseudomonas Donghuensis* Strain SVBP6. *Environ Microbiol* **2020**, *22*, 2550–2563, doi:10.1111/1462-2920.14925.
21. Pellegrini, M.; Pagnani, G.; Bernardi, M.; Mattedi, A.; Spera, D.M.; Gallo, M.D. Cell-Free Supernatants of Plant Growth-Promoting Bacteria: A Review of Their Use as Biostimulant and Microbial Biocontrol Agents in Sustainable Agriculture. *Sustainability* **2020**, *12*, 9917, doi:10.3390/su12239917.
22. Jain, R.; Pandey, A. A Phenazine-1-Carboxylic Acid Producing Polyextremophilic Pseudomonas Chlororaphis (MCC2693) Strain, Isolated from Mountain Ecosystem, Possesses Biocontrol and Plant Growth Promotion Abilities. *Microbiological Research* **2016**, *190*, 63–71, doi:10.1016/j.micres.2016.04.017.
23. Winter, N.; Trauner, D. Thiocarbonyl Ylide Chemistry Enables a Concise Synthesis of (±)-Hippolachnin A. *J. Am. Chem. Soc.* **2017**, *139*, 11706–11709, doi:10.1021/jacs.7b06815.
24. Takeshita, H.; Mori, A. An Improved Synthesis of 2,7-Dihydroxytropolone (3-Hydroxytropolone). *Synthesis* **1986**, 578–579.
25. Hamor, T.A.; Watkin, D.J. The Crystal Structure of Tris(Tropolonato)Iron(III)("Ferric Tropolone"). *J. Chem. Soc. D* **1969**, *0*, 440–441, doi:10.1039/C29690000440.
26. Jiang, Z.; Chen, M.; Yu, X.; Xie, Z. 7-Hydroxytropolone Produced and Utilized as an Iron-Scavenger by Pseudomonas Donghuensis. *Biometals* **2016**, *29*, 817–826, doi:10.1007/s10534-016-9954-0.
27. Cox, R.J.; Al-Fahad, A. Chemical Mechanisms Involved during the Biosynthesis of Tropolones. *Current Opinion in Chemical Biology* **2013**, *17*, 532–536, doi:10.1016/j.cbpa.2013.06.029.
28. Guo, H.; Roman, D.; Beemelmanns, C. Tropolone Natural Products. *Nat. Prod. Rep.* **2019**, *36*, 1137–1155, doi:10.1039/C8NP00078F.
29. Cigna, J.; Raoul des Essarts, Y.; Mondy, S.; Hélias, V.; Beury-Cirou, A.; Faure, D. Draft Genome Sequences of Pseudomonas Fluorescens Strains PA4C2 and PA3G8 and Pseudomonas Putida PA14H7, Three Biocontrol Bacteria against Dickeya Phytopathogens. *Genome Announc* **2015**, *3*, e01503-14, doi:10.1128/genomeA.01503-14.
30. Pédron, J.; Mondy, S.; Raoul des Essarts, Y.; Van Gijsegem, F.; Faure, D. Genomic and Metabolic Comparison with Dickeya Dadantii 3937 Reveals the Emerging Dickeya Solani Potato Pathogen to Display Distinctive Metabolic Activities and T5SS/T6SS-Related Toxin Repertoire. *BMC Genomics* **2014**, *15*, 283, doi:10.1186/1471-2164-15-283.
31. Haluk, J.-P.; Roussel-Bousta, C. Biosynthèse de tropolones dans les cals et les suspensions cellulaires à partir d'ébauches foliaires de plantules de *Thuja plicata* Donn. *Ann. For. Sci.* **2003**, *60*, 271–276, doi:10.1051/forest:2003018.
32. Czajkowski, R.; Pérombelon, M.C.M.; van Veen, J.A.; van der Wolf, J.M. Control of Blackleg and Tuber Soft Rot of Potato Caused by Pectobacterium and Dickeya Species: A Review. *Plant Pathology* **2011**, *60*, 999–1013, doi:10.1111/j.1365-3059.2011.02470.x.